Time-resolved optically stimulated luminescence and spectral emission features of α-Al_2O_3:C

M.L. Chithambo, A.N. Nyirenda, A.A. Finch, N.S. Rawat

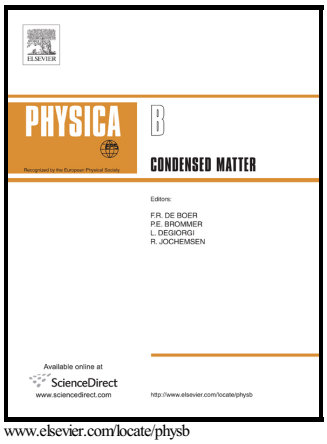

www.elsevier.com/locate/physb

PII: S0921-4526(15)30082-X
DOI: http://dx.doi.org/10.1016/j.physb.2015.05.034
Reference: PHYSB309013

To appear in: *Physica B: Physics of Condensed Matter*

Received date: 12 March 2015
Revised date: 25 May 2015
Accepted date: 26 May 2015

Cite this article as: M.L. Chithambo, A.N. Nyirenda, A.A. Finch and N.S. Rawat, Time-resolved optically stimulated luminescence and spectral emission features of α-Al_2O_3: C , *Physica B: Physics of Condensed Matter,* http://dx.doi.org/10.1016/j.physb.2015.05.034

Time-resolved optically stimulated luminescence and spectral emission features of α-Al_2O_3:C

M.L. Chithambo[a*], A.N. Nyirenda[a], A.A. Finch[b], N.S. Rawat[c]

[a]*Department of Physics and Electronics, Rhodes University, PO BOX 94, Grahamstown 6140, South Africa*
[b]*Department of Earth & Environmental Sciences, University of St Andrews, Irvine Building, St Andrews, Fife, KY16 9AL, UK*
[c]*Radiological Physics and Advisory Division, Bhabha Atomic Research Center, Mumbai -400094, India*

Abstract

This report is concerned with the influence of measurement temperature on luminescence lifetime and on the spectral emission features of luminescence from α-Al_2O_3:C. The lifetimes were determined from time-resolved luminescence spectra. Spectral measurements were done using thermoluminescence and X-ray excited optical luminescence. The emission spectra of α-Al_2O_3:C studied in this work shows prominent bands at 330, 380 and 420 nm associated with vacancies in the oxygen sub-lattice in α-Al_2O_3:C and an additional band at 695 nm due to Cr substitution for Al. Emission bands below 500 nm are independent of temperature below 125^{o}C but widen with temperature. Direct evidence of thermal quenching of the 420 nm emission band is provided. Beyond 200^{o}C, the 380 and 420 nm bands merge and widen, with the 420 nm emission dominant. Before the onset of thermal quenching, luminescence lifetimes are affected by retrapping both in the shallow- and in the main electron trap. This was deduced from features of time-resolved luminescence spectra measured from samples with and without the shallow trap. Additional measurements with temperature decreasing from 160 to 20^{o}C, after phototransfer as well as after a considerable delay between irradiation and measurement, suggest that the change in lifetimes could also be related to other factors including slight shifts in emission wavelength for the 380 and 420 nm emissions.

Keywords: Time-resolved luminescence; α-Al_2O_3:C; X-ray excited optical luminescence; lifetimes; thermoluminescence; spectra

Corresponding author. Tel.: 027 46 603 8450; fax: 027 46 603 8757.
E-mail address: m.chithambo@ru.ac.za (M.L. Chithambo).

1. Introduction

The enduring appeal of aluminum oxide (α-Al_2O_3) in defect studies is due to its peculiar luminescence properties [e.g. 1-4]. The luminescence of α-Al_2O_3 is influenced by vacancies in the oxygen sublattice. These generate colour centres notably the F and F^+ centres, that is, an oxygen vacancy with two and one electron trapped nearby respectively [3]. Optical absorption measurements show that F and F^+ centres are always present in α-Al_2O_3. The presence of the α-centre (an empty anion vacancy) has not been unequivocally established whereas the presence of colour-centre aggregates is inferred from unassigned radiative transitions [2-3].

The incorporation of carbon in α-Al_2O_3 during its synthesis to produce α-Al_2O_3:C *reduces* α-Al_2O_3 and facilitates the formation of F and F^+ centres [4-5]. These electron centres act as luminescence sites for electrons thermally or optically stimulated from electron trapping point-defects. Although α-Al_2O_3 shows emission bands at 1.25, 1.49, 3.0, 3.27 and 3.8 eV, that is, near 990, 830, 410, 380 and 330 nm respectively [2-3], the most prominent ones in α-Al_2O_3:C are near 3.0 eV (410 nm) and 3.8 eV (330 nm) respectively [4-5]. Thermoluminescence (TL) emitted near 410 nm (or variously reported as 420 nm) is attributed to intra-centre-transitions at an F centre following electron capture at an F^+ defect, whereas hole capture at an F centre or, equivalently, electron capture at an α centre accounts for the emission at 3.8 eV (330 nm) [4-6]. Whereas the features of the most prominent absorption and emission bands are well established, many other models, for example those involving hole transfer via the valence band or concentration quenching discussed elsewhere e.g. [3], have not been as well explored as have alternatives involving electron capture.

The thermoluminescence glow-curve of α-Al_2O_3:C typically consists of a prominent

glow-peak used in dosimetry and a number of weaker intensity peaks [4, 5, 7-11]. Luminescence is then discussed in terms of charge traps responsible for these peaks as well as putative deep electron- and hole-traps whose presence is deduced indirectly, for example, from induction of phototransferred thermoluminescence [12-14] or by partial heating of an irradiated sample [15]. Optically stimulated luminescence is also explained with reference to the same models as thermoluminescence [13].

The dynamics of luminescent recombination in materials including α-Al_2O_3:C can be studied using time-resolved optically stimulated luminescence (TR-OSL) in which stimulation and emission are separated in time to produce spectra that can be resolved into discrete lifetimes [16, 17]. The lifetimes denote the delay between stimulation and emission and therefore are the sum of the time to stimulate an electron bound at an electron trap, transition time through the conduction band and the relaxation time at the luminescence centre.

Markey *et al.* [18] used the 514 nm line from an argon-ion laser to pulse luminescence from α-Al_2O_3:C using pulse-widths of 10-100 ms and reported a principal lifetime of 35 ms, the intrinsic F-centre radiative emission lifetime. The same component was reported by Bulur and Göksu [19] using pulsed 565 nm green light-emitting-diodes. Time-resolved luminescence has also been measured from α-Al_2O_3:C using infrared stimulation at 880 nm by Bulur *et al.* [20] and by Bailiff and Clark [21] using 850 nm stimulation. In both cases, the principal emission was observed but with a slight offset to ~37 ms, although use of a blue detection filter by Bailiff and Clark [21] resolved the spectra to a lifetime closer to 35 ms. The influence of stimulation temperature on optically stimulated luminescence from α-Al_2O_3:C was studied by Markey *et al*. [22] using continuous optical stimulation at 500 nm as well as pulsed optical stimulation at 514 nm. These authors observed that the intensity of

optically stimulated luminescence during stimulation is temperature-dependent and that the luminescence comprises contributions from the main electron trap as well as deep traps. Further investigations in this regard but using pulsed 470 nm stimulation were reported by Pagonis *et al*. [23] and Nyirenda [24].

Time-resolved optical stimulation should not be confused with time-resolved photoluminescence (TR-PL) where excitation is performed using UV light which directly ionizes F-centres [5, 25]. Akselrod *et al.* [25] used this mode to study thermal quenching of luminescence detected at 420 nm. Pagonis *et al.* [26] referred to the model of Nikiforov *et al.* [27] and adopted suitable modifications to develop simulations of TR-PL in α-Al_2O_3:C. In their work, Pagonis *et al.* [26] developed an energy band scheme to explain thermal quenching of the 3.0 eV emission attributed to the $^3P \rightarrow {}^1S$ transition at an F centre.

The experimental features [e.g. 6, 20-25] suggest that although luminescence from α-Al_2O_3:C has multiple sources [3, 28], the contribution from the F-centre is dominant. This is particularly evident when the emission is measured as a thermoluminescence isometric plot above ambient temperature [29, 30]. In addition, excitation at UV wavelengths discriminates against other emissions except the F-centre one and thus fine features involving other transitions are usually too faint to be instructive.

The third type of luminescence used in this study, X-ray excited optical luminescence (XEOL, often referred to as radioluminescence (RL)) is the luminescence emitted during X-ray irradiation. Since the luminescence is measured as a function of the emission wavelength, the method provides a means to measure the nature of the emission band and how this is affected by dopants [31], impurities [32], irradiation dose [33], or pre-irradiation

annealing [34, 35]. XEOL was used to study the effect of both X-ray dose and measurement temperature on the emission bands.

This report is therefore concerned with the influence of measurement temperature on luminescence lifetimes and the spectral emission features of luminescence from α-Al_2O_3:C. The lifetimes were determined from time-resolved optically stimulated luminescence (TR-OSL) spectra. On the other hand, emission spectra were measured both during and after irradiation to better examine the temperature dependence of various emission bands in α-Al_2O_3:C.

2. Experimental details

2.1 Measurement of time-resolved luminescence spectra

Measurements were made on α-Al_2O_3:C single crystal discs of 5 mm diameter and 1 mm thickness (Rexon TLD Systems, Ohio, USA). Samples were annealed once at 900^{o}C for 15 minutes before use to remove any residual charge from deep traps. Samples were irradiated at ambient temperature using a $^{90}Sr/^{90}Y$ β-source at a dose rate of 0.10 Gy s^{-1}.

TR-OSL was measured using a light-emitting-diode (LED) based pulsing system [36, 37]. In the system, an ORTEC MCS-plus multichannel scaler is used to trigger a set of LEDs at preset repetition rates while simultaneously processing resultant luminescence photon counts from an EMI 9635QA photomultiplier to produce TR-OSL. The multichannel scaler records photon counts sequentially in the selected channels of its memory advancing with negligible

dead-time between channels and sweeps. The time-resolved spectrum measured in this way is a distribution of cumulative photon counts against time for the dynamic range selected.

Luminescence was stimulated at a pulse-width of 16 ms using a set of 470 nm blue LEDs (Nichia NSPB-500) and detected between 340-380 nm through a combination of Schott BG39 and UG11 filters. Each time-resolved spectrum was obtained using 100 sweeps, dwell time of 1 ms and a dynamic range of 500 ms. The measurement temperature was controlled by an AO500 sample heater (MBE-Komponenten GmbH, Germany) with the sample-stage being a ceramic thin-film heater plate, driven by direct-current, and fitted with a PT100 temperature sensor. Unless otherwise specified, all data in this report is presented in degrees Celcius.

An example of a time-resolved spectrum from α-Al_2O_3:C measured at 40℃ is shown in Fig. 1. The signal build-up during pulsing includes a monotonically increasing luminescence component whereas after the light pulse, the luminescence decreases in time over background. The background, shown for comparison, consists of photomultiplier noise and stimulating light scattered off a blank stainless steel sample disk during stimulation but photomultiplier noise only after the light pulse.

Luminescence lifetimes were evaluated from the portion of each time-resolved spectrum after the pulse by fitting exponential functions of the form

$$f(t) = A\exp(-t/\tau) + B, \qquad (1)$$

where τ is the lifetime, A is a scaling factor, t is time. The uncertainty $\Delta\tau$ in the lifetime reflects the scatter in data points in the time-resolved spectrum used to evaluate the lifetime. In studies on quartz e.g. [16, 17, 38] the parameter B denotes the background. However, in α-Al_2O_3:C, B is known to be a temperature-dependent phosphorescence component with a lifetime of several hundred milliseconds [23, 25]. This work, for which the dynamic range was only 500 ms, is not concerned with this term.

The solid line through data after the light-pulse in Fig. 1 is the best fit of Eq. (1) giving a lifetime of value 35.6 $\pm$ 0.1 ms. This is consistent with the main lifetime in α-Al_2O_3:C (~35 ms), attributed to the $^3P \rightarrow {}^1S$ transition at an excited F-centre [4, 5].

2.2 Measurement of luminescence spectral emission

The study using time-resolved optical stimulation was supplemented by spectral measurements of thermoluminescence as well as X-ray excited optical luminescence (XEOL). The purpose of the XEOL and TL measurements was to obtain more comprehensive details on the dynamics involved in the luminescence which is possible when the signal is recorded as an emission spectrum to reveal information not only concerning the electron traps but about luminescence sites as well e.g. [31, 39, 40].

XEOL measurements were made in ~1 mbar vacuum either at room temperature or by ramping to 400°C at 10 K min^{-1} using an upgraded version of the high sensitivity thermoluminescence spectrometer described by Luff and Townsend [41]. Samples were irradiated *in-situ* with X-rays from a Philips MCN-101 X-ray tube operated at 20 kV/4 mA giving a dose rate of 1.8 Gy min^{-1}. For XEOL, the data are collected during irradiation and

temperature ramping in real time, whereas for TL the sample is irradiated and the irradiation stopped prior to ramping.

The luminescence detection system consists of a combination of two spectrometers capable of recording emissions over the wavelength range 250 to 850 nm. A diagram of the light collection optics is shown in Fig. 2. Two grating spectrometers diffract the incoming light onto position sensitive imaging plate detectors and the position of the photon on the plate is converted to a spectrum. The gratings, one at each detector, disperse the signal across the relevant range *i.e.* 250-550 nm and 380-850 nm. All spectral data are corrected for the wavelength response of the system. 0.5 mm entrance slits were used on the spectrometers giving a typical 5 nm resolution over the whole wavelength range. A 400 nm cut-off filter is inserted in the light path to the 380-850 nm detector to remove the second order scattering of lower wavelengths into the first-order spectrum. In measurements of thermoluminescence and temperature-dependence of XEOL, a temperature scan was obtained every 5 K equivalent to a spectrum recorded every 30 s. Spectral data were corrected for dark current and subsequently smoothed in wavelength using a three point running mean.

3. Results and discussion

3.1 Thermoluminescence glow-curves

Examples of thermoluminescence glow-curves from α-Al_2O_3:C studied are shown in Fig. 3. Two types of TL responses were noted. For some samples, the glow-curve consists of the main peak flanked by a number of weaker intensity ones below and above 200^{o}C (Fig. 3, open circles). Other samples, from the same batch, showed similar features except the shallow trap (Fig. 3, solid circles). For ease of reference, samples with the shallow trap, or

peak I, are labelled type A and those without, type B. It is now known that the main peak (peak II) is collocated with a weaker-intensity component (peak IIA) on its higher temperature end [9]. It should be noted that Fig. 3 is only included to distinguish between type A and B samples, for reference later in the text, and not for kinetic analysis.

3.2 Measurement temperature and time-resolved luminescence spectra

3.2.1 Temperature dependence of luminescence lifetimes: Influence of shallow traps and retrapping

The temperature dependence of luminescence lifetime was studied for measurements made at 10^{o}C intervals between 20 and 200^{o}C. Before each measurement, an allowance was made for the sample to come to temperature. Unless otherwise stated, each sample was irradiated only once to 1 Gy prior to use and not irradiated again between measurements. Figure 4 compares the temperature dependent change of lifetimes in sample types A and B.

Figure 4 (solid circles) shows the change of lifetimes with temperature for a sample irradiated to 1 Gy. The lifetimes increase from 34.8 ± 0.1 ms to 35.6 ± 0.1 ms between 20 and 40^{o}C and then decrease to 34.8 ±0.1 ms when the temperature is increased to 60^{o}C. Between 60 and 120^{o}C, the lifetimes go through another peak with temperature and then decrease consistently to 23.9 ± 2.0 ms at 160^{o}C. The lifetime dependence on temperature, with the double peak (Fig. 4, solid circles) is unlike any other reported for α-Al_2O_3:C e.g. [23, 25] where only the initial peak feature (between 20 and 60^{o}C in Fig. 4) was observed and attributed to re-trapping in the shallow trap. This model is confirmed by measurements in a type B sample (inset to Fig. 4) where the initial peak in lifetimes is less pronounced although not completely absent. It is reasonable to deduce that the absence of the initial peak in type B α-$A1_2O_3$:C does not necessarily imply the absence of the electron traps responsible. Instead, this may only indicate a significantly reduced concentration in the associated point defects in

comparison with that in type A samples. On the other hand, we attribute the peak in lifetimes between 60 and 120^{o}C to retrapping in the electron trap responsible for the main peak.

3.2.2 Further investigations of retrapping and lifetimes

The possibility that re-trapping may extend lifetimes was examined further by (a) delaying (for 14 hours) the start of measurement after irradiation, (b) recording time-resolved spectra after the sample had been briefly pre-exposed to 470 nm light, or (c) monitoring the temperature-dependence of lifetimes with the temperature decreasing from a high value to ambient. These protocols were followed for several reasons. Some studies e.g. Chithambo and Seneza [8] have shown that the loss of signal from the shallow trap (peak I in Fig. 3) by phosphorescence is accompanied by a concomitant increase of TL intensity from the main trap (peak II) and other higher temperature peaks. Thus in principle, delaying measurement after irradiation should act as a way of filling the main- and other higher temperature electron traps thereby decreasing incidences of retrapping. Alternatively, pre-exposing an irradiated sample to 470 nm stimulating light under steady-state conditions prior to TR-OSL measurement should ensure that electrons are moved, by phototransfer, from deep to shallower electron traps involved in the OSL process and thereby also reduce retrapping. The third option with the temperature decreasing is intended to avoid any retrapping at all.

Figure 5 shows the temperature dependence of lifetimes corresponding to a 14-hour delay after irradiation (solid squares) and after phototransfer (open squares). Although the lifetimes still slightly increase in the temperature vicinity of the shallow and main traps, the effect is now significantly less than before. The profile of the change is similar in both cases with lifetimes scattering about 35 ms between 20 and 120^{o}C and decreasing to about 12 ms at 170^{o}C. The influence of the shallow and main electron trap on lifetimes was further studied in measurements made from 160 to 20^{o}C (inset, Fig. 5). In this procedure, there should be

negligible retrapping in these putative competitor traps. However, as is apparent in Fig. 5 (inset), the lifetimes still increase in the regions associated with the shallow and main electron traps. This is counter-intuitive since retrapping should be less effective when the temperature is decreased from a high value to ambient. Our conclusion is that the change of lifetimes as observed may not be due to retrapping alone but could also be caused by other factors including slight shifts in emission wavelength. This will be examined further later in the text.

3.2.3 Analysis using the signal during stimulation

Luminescence lifetimes described earlier were found using the portion after the light pulse using Eq. (1). However since the physical processes of luminescence during and after the light-pulse are identical, lifetimes can also be abstracted from the portion of the time-resolved spectrum during stimulation using functions of form

$$f(t) = \kappa[1 - \exp\left(-\frac{t}{\tau}\right)], \qquad (2)$$

where κ is a scaling factor, t the time and τ the lifetime [16, 17]. Figure 6 shows lifetimes found this way from type A and B samples. The data show the influence of the shallow trap on lifetime as presumed previously. Again the margin of error in the lifetime simply reflects the scatter in data points in the associated TR-OSL spectrum. Except for Fig. 6, all lifetimes were found from the portion after the light pulse. The results in Figs. 4-6 suggest that models of stimulated luminescence in α-Al_2O_3:C should be based on non-negligible retrapping.

3.2.4. Thermal quenching

The temperature induced decrease of lifetimes in Figs. 4-6 is evidence of thermal quenching of the associated luminescence. This feature was used to evaluate the activation energy of thermal quenching. For type B samples, the change of lifetime with temperature *τ(T)* better follows the usual behaviour as

$$\tau(T) = \frac{\tau_{rad}}{1+Cexp(-\Delta E/kT)}, \qquad (3)$$

where *T* is the absolute temperature, τ_{rad} is the radiative lifetime at 0 K, ΔE is the activation energy for thermal quenching, *k* is Boltzmann's constant and the constant *C* is equal to $\nu\tau_{rad}$ where ν is the frequency factor for the non-radiative process [2, 17]. The solid line through data in Fig. 4 (inset) and Fig. 6 is in each case the best fit of Eq. (3) giving ΔE = 1.025 ± 0.002 eV and ΔE = 1.011 ± 0.005 eV respectively. The values are consistent as expected. The parameter C was found in each case as 2.14 x10^{11} from which $\nu = (6.00 \pm 0.05) \times 10^{12}$ s^{-1} for Fig. 4 (inset) and $\nu = (5.50 \pm 0.10) \times 10^{12}$ s^{-1} corresponding to Fig. 6 (inset). In comparison, Akselrod *et al.* [25] reported $\Delta E = 1.08 \pm 0.03$ eV and $\nu = (1.02 \pm 0.84) \times 10^{14}$ s^{-1}. In our calculations, the value of τ_{rad} used was that obtained from the nonlinear regression and not the intrinsic 35 ms as done by Akselrod *et al.* [25]. We interpret ν as the number of times an electron in the excited state attempts to escape its binding potential by phonon transition between vibrational levels. The results of Figs. 4-6 suggest that unless a sample has very low concentration of shallow traps or negligible retrapping applies, Eq. (3) is only approximate. An exact mathematical form for the experimental behaviour is still outstanding.

3.2.5. Nature of electron traps in a-Al_2O_3:C

Identification of electron traps in α-Al_2O_3:C was outside the scope of this work but some remarks can be made. Although α-Al_2O_3:C contains many impurities [4], the role of carbon

in the luminescence is central. One theory is that the replacement of Al^{3+} by C^{2+} promotes the formation of F^+ centres thereby improving the TL sensitivity. In particular, the F^+ is linked to the high intensity of the main peak seen near 200^{o}C. In a study on electronic properties of carbon in α-Al_2O_3:C, Zhu et *al*. [42] reported that C preferentially occupies the Al site under O-rich conditions whereas when Al is in greater concentration, C tends to occupy the O site. Zhu et al. [42] deduced that carbon at an Al site (C_{Al}), with an associated energy level close to the conduction band minimum, can serve as an electron trap. Kinetic analysis shows that the kinetic energy of peak I is equal to 0.72±0.05 eV [9] or similar [8, 18], the least for all peaks in α-Al_2O_3:C. We therefore conclude that the electron trap responsible for peak I is consistent with the C_{Al} site. Further, different concentrations of C_{Al} in the material could account for the existence of types A and B samples.

3.3 Luminescence spectra

3.3.1 Thermoluminescence spectra

Since lifetimes in α-Al_2O_3:C change with temperature (Figs. 4-6), investigations were done to assess whether the corresponding emission spectra are similarly affected, and if so, its bearing on interpretation of mechanisms of the luminescence. Emission spectra were measured using thermoluminescence and X-ray excited optical luminescence.

Figure 7 shows contour maps of thermoluminescence measured between 25 and 400^{o}C at 10 K/min from X-ray irradiated α-Al_2O_3:C. Figure 7(a), for irradiation to 1 Gy, shows a prominent emission band, as expected, centred near 420 nm at 160^{o}C. Its extreme intensity causes any other fine details of the emission spectrum to be concealed. Figure 7(b), an isometric plot measured after 10 Gy irradiation, shows the emission band to have widened owing to an increase in intensity of wavelength components above and below 420 nm. The position of the band has also shifted with dose to about 450 nm. In principle, it is known that

different emission features induced by oxygen vacancies change with dose at different rates [2]. The presence of other TL peaks in Figs. 7(a) and (b) beyond the main one is not obvious.

The emission spectrum was then examined using measurement only up to 100^{o}C (Figs. 7(c)) to emphasize the features of the shallow trap responsible for peak I. It is evident that peak I and the main TL peak correspond to the same emission wavelength. In comparison, the spectral measurements of Akselrod and Kortov [43], where the photon energy was plotted in lieu of wavelength as a function of temperature, showed a dominant emission band at about 3.0 eV (i.e. 420 nm) but not the number of TL peaks associated with a particular band.

3.3.2 X-ray excited optical-luminescence spectra

The emission was further studied using X-ray excited optical-luminescence (XEOL) by monitoring the emission wavelength at different temperatures. Figure 8(a) shows an XEOL spectrum obtained at room temperature using an integration time of 30 s. The spectrum shows three bands, near 330, 380 and 420 nm and an unresolved band near 440 nm. Figures 7 and 8(a) shows that stimulated luminescence from α-Al_2O_3:C is emitted simultaneously at 330, 380 and 420 nm from at least 3 types of recombination centres. This data also shows that the position of the emission bands is affected by temperature and dose.

When XEOL is instead recorded as a function of temperature, several important features emerge, as evident in Fig. 8(b), an XEOL isometric plot measured up to 100^{o}C, that is, before the onset of the main glow peak. The plot shows the three bands below 450 nm mentioned earlier and an additional narrow one at ~695 nm too faint to appear in Figs. 7 and 8(a). The 695 nm emission is also an example of stimulated luminescence. Fig. 8 shows distinct emission bands which are otherwise masked by higher temperature glow-peaks emitting below 450 nm when the spectrum is measured under TL and secondly, that all the bands are

independent of temperature, at least up to 100°C studied here. For ease of reference, the emission bands at 330, 380, 420 and 695 nm will be labelled K, L, M and N respectively.

Figure 9 shows XEOL measured at 10 K/min from 25 to 400°C. Two different perspectives of the isometric plot are shown in Figs. 9(a) and (b) and the corresponding contour map in Fig. 9(c). The isometric plot shows, in the initial stages of measurement, clear emission bands at 380 and 420 nm whereas the bands at 330 nm and 695 nm are just perceptible. In general, the emission appears as a collection of broad overlapping bands rather than as sharp line structures as evident in, for example, calcite and related materials with low concentration of Mn^{2+} cations [40, 44].

Figure 9 shows that the emission bands at 330, 380 and 420 nm are independent of temperature up to about 125°C. In particular, the width of band M (at 420 nm) is independent of temperature particularly up to 125°C (Fig. 9c). A notable feature of the emission spectrum spanning 140-190°C and centred near 425 nm is the significant decrease of luminescence intensity. This is direct evidence of the well documented [9, 23, 25] thermal quenching of the '420 nm' emission band. Subsequently, between 190 and 200°C, the band narrows and its wavelength decreases slightly away from 420 nm. The other subtle changes in emission wavelength and bandwidth during this process are less well known.

The emission band at 380 nm (band L) is also independent of temperature up to about 125°C. Between 125°C and 175°C, its width decreases. Fig. 9(b) also shows that beyond 200°C bands L and M merge and widen with band M dominant. The emission from band K (at 330 nm) is too faint for its features to properly emerge but that at 695 nm is independent of temperature.

3.3.3 Interpretation of spectral features: General observations

Luminescence emission bands in corundum (Al_2O_3) are associated with oxygen vacancies or their clusters [1, 2, 6]. The incorporation of carbon in Al_2O_3 to produce α-Al_2O_3:C increases the concentration of colour centres but does not seem to introduce new emission bands. The previous section showed a number of features some of which have been observed or noted before in principle e.g. evidence of change of wavelength of the main band with temperature [3, 43] and, thermal quenching [4, 6]. An exhaustive account of the characteristics is outside the scope of this study. However, since the results have a bearing on TR-OSL spectra, some propositions on the observed aspects of emission features related to oxygen vacancies will be made.

Figs. 7 and 8, show that if an isometric plot is measured using thermoluminescence from, say 20 to 400^{o}C, all detail in emission characteristics is lost since the spectrum is dominated by the main TL peak. This has also been acknowledged by Yukihara and McKeever [5].

The emission spectra of α-Al_2O_3:C studied in this work shows five emission bands near 330, 380, 420, 440 associated with vacancies in the oxygen sub-lattice and 695 nm attributed to Cr impurities [2, 6]. The characteristics of these bands are further explained with reference to Fig. 10 which shows possible transitions at colour centres in α-Al_2O_3:C. The main absorption band is seen at 6.03 eV and is attributed to a transition from the ^{1}S ground state to the ^{1}P excited state at an F-centre [2, 4, 45]. The energy levels are not intrinsic to the F-centre but rather are based on an analogue system, an He-2 atom. Although the 6.03 eV transition is typically shown as single, some experimental data show that this band is in fact composite e.g. Agullo-Lopez et al. [2], their Fig 6.5. The excited ^{1}P level in Fig. 10 is set in the conduction band here and elsewhere e.g. Vinceller et al. [46] because the F band is known to show photocurrents down to 10 K [2, 47]. The emission at 3.0 eV (420 nm) is generated by the transition from the ^{3}P excited state to the ^{1}S ground state [2, 4, 48].

The emission at 3.76 eV (330 nm) is ascribed to a transition from the 1B excited state to the 1A ground state at an F^+ centre [2]. The F^+ point-defect is distinguished from the F colour centre because the F^+ has a 3-fold degenerate excited state and thus shows three distinct absorption bands at 6.3, 5.41 and 4.84 eV [2, 4, 49]. The emission at 380 nm (3.27 eV) has been linked to an F_2 centre, that is, a pair of adjacent F centres [2]. Other possibilities have been reviewed elsewhere [1-6].

The luminescence emitted at 695 nm has been observed before in Cr-doped Al_2O_3 [6, 50] as well as in Cr-doped beryl [31]. This emission is associated with Cr^{3+} which substitutes homovalently for Al^{3+}. However, since the size of Cr, at 0.63 Å, is much larger than that of Al, at 0.51 Å, the substitution distorts the structure of the host. The emission can be discussed with reference to a configurational coordinate diagram of a Cr^{3+}cation in a site of high crystal strength, relevant in this discussion [1, 51]. The emission spectrum of Cr^{3+} consists of a sharp doublet denoted R_1 and R_2. The doublet is not obvious in Fig. 8(b) measured at high temperature but better apparent at low temperature [31]. The R lines are due to the transitions $^2E \rightarrow {}^4A_2$ with the ^2E level being two fold degenerate. The emission appears as a broad band in Fig. 8(b) because it is a composite of the transitions $^2E \rightarrow {}^4A_2$ and $^4T_2 \rightarrow {}^4A_2$ with the latter being dominant. The Cr^{3+} emission in beryl was similarly explained [31]. In general, the energy level diagram of an isolated ion is modified when the ion is incorporated in a host structure e.g. [40].

3.3.4 The influence of temperature on width, intensity and position of emission bands

The temperature-dependent increase of width of bands L (at 380 nm) and M (at 420 nm) may be due to the F centre being strongly coupled to the lattice. According to the semiclassical configurational coordinate model, the band width at high temperature can be approximated as

$$\Delta W(T) \approx \Delta W_o \left(\frac{2k}{\hbar\omega}\right)^{1/2} T^{1/2}, \qquad (4)$$

where ΔW_o is the width at absolute zero of temperature, k is Boltzmann's constant and $\hbar\omega$ is the energy of the coupling phonon. Increase in the width of each band therefore accentuates the overall width of the region of overlap of the bands as evident in Fig. 9(b).

The change in position and intensity of emission bands L (at 380 nm) and M (at 420 nm), including the complete loss in emission at 140-190^{o}C/425 nm may be accounted for with reference to the configurational coordinate diagrams shown in Fig. 11. A detailed explanation of non-radiative transitions in terms of such diagrams is given elsewhere e.g. [1, 2, 51-53] hence only a brief qualitative account of specific results in this work is given here. The diagrams in Fig. 11 correspond to strong electron-lattice coupling hence the adiabatic potential energy curves have been drawn to intersect at point P. In both diagrams, state B corresponds to maximum absorption. The probability of de-excitation of an electron in an excited state consists of a multiphonon relaxation term (transition 1; Fig. 11a) to state C from which radiative emission (transition 2) occurs followed by another multiphonon down-relaxation to state A (transition 3), corresponding to the equilibrium position $q_o^{(g)}$. If, however, point P is at a lower energy than state B, the electron can down-relax to the vibrational state corresponding to point P (transition 1`, Fig. 11(b)) which is now degenerate to both the ground and the excited states. In this case, the vibrational state corresponding to point C is not occupied and thus the de-excitation probability is much greater by way of

phonon states of initial state g (transition 5; Fig. 11(b)) than of state e thus no luminescence occurs [1, 52, 53].

It can be deduced from Fig. 11(a) that the overall probability of de-excitation has radiative, multiphonon down-transition and multiphonon non-radiative terms as

$$\frac{1}{\tau} = \frac{1}{\tau_{rad}} + \gamma coth\left(\frac{\hbar\omega}{kT}\right) + \nu \exp\left(\frac{-\Delta E}{kT}\right), \qquad (5)$$

where τ is the lifetime of the excited state, τ_{rad} is the radiative lifetime at absolute zero of temperature, γ is a constant, $\hbar\omega$ and ΔE and ν are as previously defined [2].

In view of the discussions above, the shift in emission wavelength in Fig. 9 could be caused by a temperature-induced offset of state e from its equilibrium coordinate $q_o^{(e)}$ such that the magnitude of transition 2 changes. Another possible cause could be formation of F-centre aggregates, which along the lines of Mollwo-Ivey law [54], the potential that the trapped electron sees is spread over a large area such that the transition energies between electronic states become altered. On the other hand, the decrease of luminescence intensity with temperature is attributed to increased probability of multi-phonon emission (transition 5).

4. Conclusions

The influence of measurement temperature on luminescence lifetimes determined from time resolved spectra as well as thermoluminescence and XEOL spectra from α-Al_2O_3:C has been investigated. Before the onset of thermal quenching, the lifetimes are affected by retrapping both in the shallow and in the main electron trap. That this is the case was concluded from features of time-resolved spectra measured from samples with and without the shallow trap. Additional measurements with the temperature decreasing from 160 to 20^{o}C; after phototransfer as well as after a considerable delay between irradiation and measurement

suggest that the change of lifetimes could also be caused by other factors including slight shifts in emission wavelength. The emission spectra of α-Al_2O_3:C studied in this work shows five emission bands at 330, 360, 420, 440 and 695 nm. The emission at 330, 380 and 420 nm are each associated with vacancies in the oxygen sub-lattice in α-Al_2O_3:C whereas that at 695 nm is attributed to Cr impurities. Emission bands below 440 nm are independent of temperature below 125^{o}C beyond which their width changes. We have provided direct evidence of thermal quenching for the 420 nm emission at 160^{o}C. Beyond 200^{o}C, the 380 and 420 nm bands merge and widen, with the 420 nm emission dominant. The intensity of the F^{+} band at 330 nm was too low to decide whether it is also affected by thermal quenching. An important conclusion from this study is that the emission from α-Al_2O_3:C has simultaneous contributions from at least five emission bands and that, although the one near 420 nm is dominant at ambient temperature, changes in various parameters such as lifetimes with temperature cannot be attributed to retrapping or dose alone. It is inferred that these are also subject to interaction of point-defects in the material.

Acknowledgements

We acknowledge, with gratitude, financial support from Rhodes University and the National Research Foundation of South Africa (Grant UID 87358).

References

1. B. Henderson, G.F Imbusch, Optical spectroscopy of inorganic solids (reprint), Oxford Science Publications, Oxford, 2006.
2. F. Agullo-Lopez, C.R.A. Catlow, P.D. Townsend, Point defects in materials, Academic Press, London, 1988.
3. B.D. Evans, J. Nucl. Mater. 219 (1995) 202.
4. S.W.S. McKeever, M. Moscovitch, P.D. Townsend, Thermoluminescence dosimetry materials: properties and uses, Nuclear Technology Publishing, Kent, 1995.
5. E.G. Yukihara, S.W.S McKeever, Optically stimulated luminescence: Fundamentals and Applications, Wiley, New York, 2011.
6. G.P. Summers, Radiat. Prot. Dosim. 8 (1984) 69.
7. M.L. Chithambo, South Afric. Journ. Sci. 100 (2004) 1.
8. M.L. Chithambo, C. Seneza, Physica B: Condens. Matter. 439 **(**2014) 165.
9. M.L. Chithambo, C. Seneza, F.O. Ogundare, Radiat. Meas. 66 (2014) 21.
10. V.S. Kortov, I.I. Milman, E.V. Moiseykin, S.V. Nikiforov, M.M. Ovchinnikov, Radiat. Prot. Dosim. 199 (2006) 41.
11. D.R. Mishra, M.S. Kulkarni, K.P. Muthe, C. Thinaharan, M. Roy, S.K. Kulshreshtha, S. Kannan, B.C. Bhatt, S.K. Gupta, D.N. Sharma, Radiat. Meas. 42 (2007) 170.
12. E. Bulur, H.Y. Göksu, Radiat. Meas. 30 (1999) 203.
13. L. Bøtter-Jensen, S.W.S. McKeever, A.G. Wintle, Optically Stimulated Luminescence Dosimetry, Elsevier, Amsterdam, 2003.
14. C. Seneza, Thermoluminescence of secondary glow peaks in carbon-doped aluminium oxide, Unpublished MSc thesis, 2014.
15. E.G. Yukihara, V.H. Whitley, J.C. Polf, D.M. Klein, S.W.S. McKeever, A.E. Akselrod, M.S. Akselrod, Radiat. Meas. 37 (2003) 627.

16. M.L. Chithambo, J. Phys. D.: Appl. Phys. 40 (2007) 1874.

17. M.L. Chithambo, J. Phys. D.: Appl. Phys. 40 (2007) 1880.

18. B.G. Markey, L.E. Colyott, S.W.S. Mckeever, Radiat. Meas. 24 (1995) 457.

19. E. Bulur, H.Y. Göksu, Radiat. Meas. 27 (1997) 479.

20. E. Bulur, H.Y. Göksu, Radiat. Meas. 29 (1998) 625.

21. I.K. Bailiff, R.J. Clark, Radiat. Prot. Dosim. 84 (1999) 457.

22. B.G. Markey, S.W.S. McKeever, M.S. Akselrod, L. Bøtter-Jensen, N. Agersnap-Larsen, L.E. Colyott, Radiat. Prot. Dosim. 65 (1996) 185.

23. V. Pagonis, C. Ankjaergaard, M. Jain, R. Chen, J. Lumin. 136 (2013) 270.

24. Nyirenda, Mechanisms of luminescence in α-Al_2O_3: C: Investigations using time-resolved optical stimulation and thermoluminescence techniques, Unpublished MSc thesis, 2013.

25. M.S. Akselrod, N. Agersnap-Larsen, V. Whitley, S.W.S. McKeever, J. Appl. Phys. 84 (1998) 3364.

26. V. Pagonis, R. Chen, J.W. Maddrey, B. Sapp, J. Lumin. 131 (2011) 1086.

27. S.V. Nikiforov, I.I. Milman, V.S. Kortov, Radiat. Meas. 33 (2001) 547.

28. B.D. Evans, G.J. Pogatshnik, Y. Chen, Nucl. Instrum. Meth. B. 91 (1994) 258.

29. V.H. Whitley, S.W.S. McKeever, J. Appl. Phys. 87 (2000) 249.

30. S.W.S. Mckeever, M.S. Akselrod, L.E. Colyott, N. Agersnap Larsen, J.C. Polf, V. Whitley, Radiat. Prot. Dosim. 84 (1999) 163.

31. M.L. Chithambo, S.G. Raymond, T. Calderon, P.D. Townsend, J. African Earth Sci. 20 (1995) 53.

32. M. Martini,M. Fasoli, I. Villa, P. Guibert, Radiat. Meas. 47 (2012) 846.

33. G.E. King, A.A. Finch, R.A.J. Robinson, R.P. Taylor, J.F.W. Mosselmans, Radiat. Meas. 46 (2011) 1082.

34. S.W.S. McKeever, J.A. Strain, P.D. Townsend, P. Uvdal, Eur. PACT J. 9 (1983) 123.

35. V. Pagonis, M.L. Chithambo, R. Chen, A. Chruścińska, M. Fasoli, S.H. Li, M. Martini, K. Ramseyer, J. Lumin. 145 (2014) 38.

36. M.L. Chithambo, J. Lumin. 131 (2011) 92.

37. M.L. Chithambo, R.B. Galloway, Meas. Sci. Technol. 11 (2000) 418.

38. R.B. Galloway, Radiat. Meas. 35 (2002) 67.

39. P.D. Townsend, Y. Kirsh, J. Contemp. Phys. 30 (1989) 337.

40. P.D. Townsend, B.J. Luff, R.A. Wood, Radiat. Meas. 23 (1994) 433.

41. B.J. Luff, P.D. Townsend, Meas. Sci. Technol. 4 (1993) 65.

42. M.S. Akselrod, V.S. Kortov, Radiat. Prot. Dosim. 33 (1990) 123.

43. J. Zhu, K.P. Muthe, R. Pandey, J. Phys. Chem. Sol 75 (2014) 379.

44. M.L. Chithambo, V. Pagonis, F.O. Ogundare, J. Lumin. 145 (2014) 180.

45. R.D. Evans, M. Stapelbroek, Phys. Rev B. 18 (1978) 7089.

46. S. Vinceller, G. Molnar, A. Berkane-Krachai, P. Iacconi, Radiat. Prot. Dosim. 100 (2002) 79.

47. B.G. Draeger, G.P. Summers, Phys. Rev. B 19 (1979) 1172.

48. J.D. Brewer, B.T. Jeffries, G.P. Summers, Phys. Rev. B 22 (1980) 4900.

49. S.Y. La, R.H Bartram, R.T Cox, J. Phys. Chem. Solids 34 (1973) 1079-1086.

50. P.J. Chandler, P.D. Townsend, Radiat. Eff. Defect. Solid. 43 (1979) 61.

51. M. Gaft, R. Reisfeld, G. Panczer, Modern luminescence spectroscopy of minerals and materials, Springer, Berlin, 2005.

52. J. Garcià Solé, L.E. Bausà, D. Jaque, An introduction to the optical spectroscopy of inorganic solids, Wiley, New York, 2005.

53. M. Fox, Optical Properties of Solids, Oxford University Press, Oxford, 2001.

54. N.W. Ashcroft, N.D. Mermin, Solid State Physics, Saunders College, Philadelphia, 1975.

Figure and table captions

Figure 1 A time-resolved spectrum from α-Al_2O_3:C irradiated to 1 Gy measured at 40°C over 100 sweeps at a pulse-width of 16 ms per sweep and a dynamic range of 500 ms. The background signal (scaled up 20x for visual clarity) is shown for comparison.

Figure 2 A schematic diagram of the luminescence spectrometer. Luminescence is collected by the pair of lenses, dispersed by the pair of grating spectrometers and detected by two position sensitive photomultiplier tubes.

Figure 3 A comparison of thermoluminescence glow-curves measured from a sample with a shallow trap (open circles) and another where this is absent. The measurements were in each case made at 1^oCs^{-1} after irradiation to 1 Gy.

Figure 4 The influence of measurement temperature on lifetimes in a sample with shallow traps (solid circles) and in one without (inset).

Figure 5 A comparison of the temperature dependence of lifetimes after fading (solid squares) and phototransfer (open squares). The inset shows results of measurements immediately after irradiation made from 160 to 20°C.

Figure 6 A comparison of luminescence lifetimes in type A and B samples of α-Al_2O_3:C for lifetimes calculated using the portion of the time-resolved spectrum during the light pulse.

Figure 7 Contour maps of TL from α-Al_2O_3:C beta irradiated to 1 Gy (a) 10 Gy (b) and 1 Gy but measured up to 100°C (c).

Figure 8 An XEOL spectrum measured at room temperature using an integration time of 30 s (a) and an XEOL contour map measured up to 100°C. The data has been corrected for blackbody radiation.

Figure 9 The temperature-dependence of XEOL (a and b) and the corresponding contour map (c). The small feature observed at 800 nm that follows the profile of the strong ~400 nm emission data is only an experimental artefact caused by second order diffractions

Figure 10 Energy band scheme for various transitions in α-Al_2O_3:C.

Figure 11 Configurational coordinate diagram to explain radiative transitions (a) and non-radiative processes (b).

Figure 1

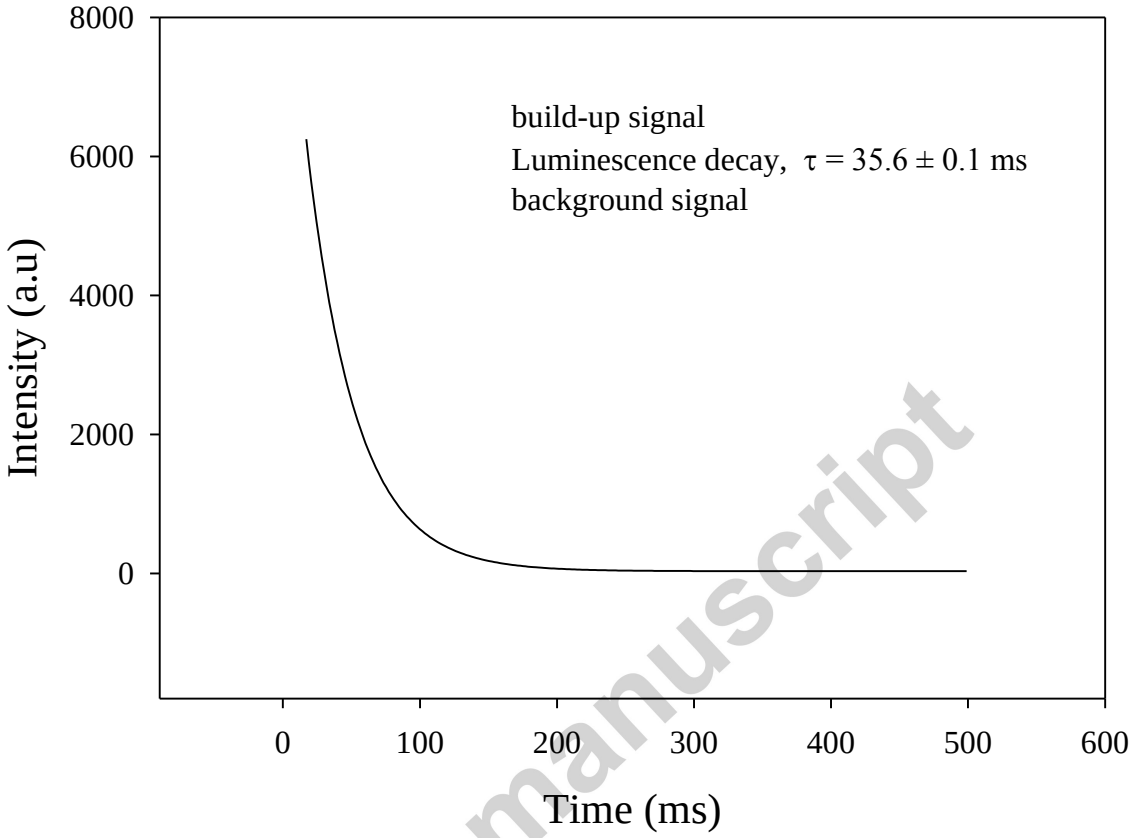

Figure 2

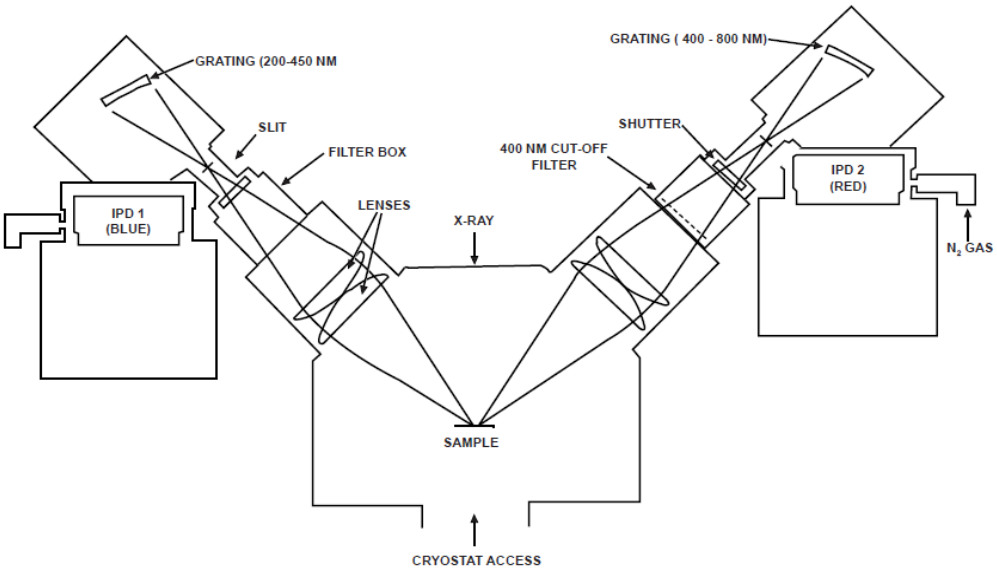

Figure 3

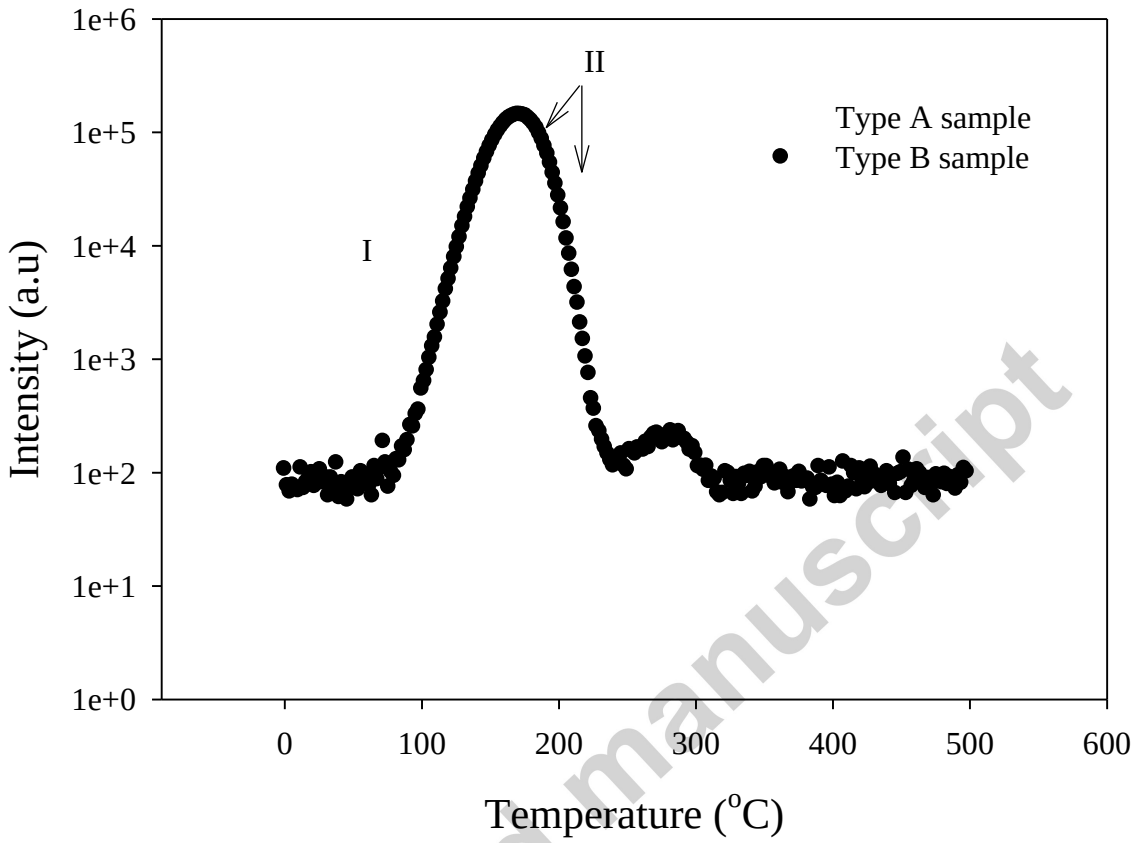

Figure 4

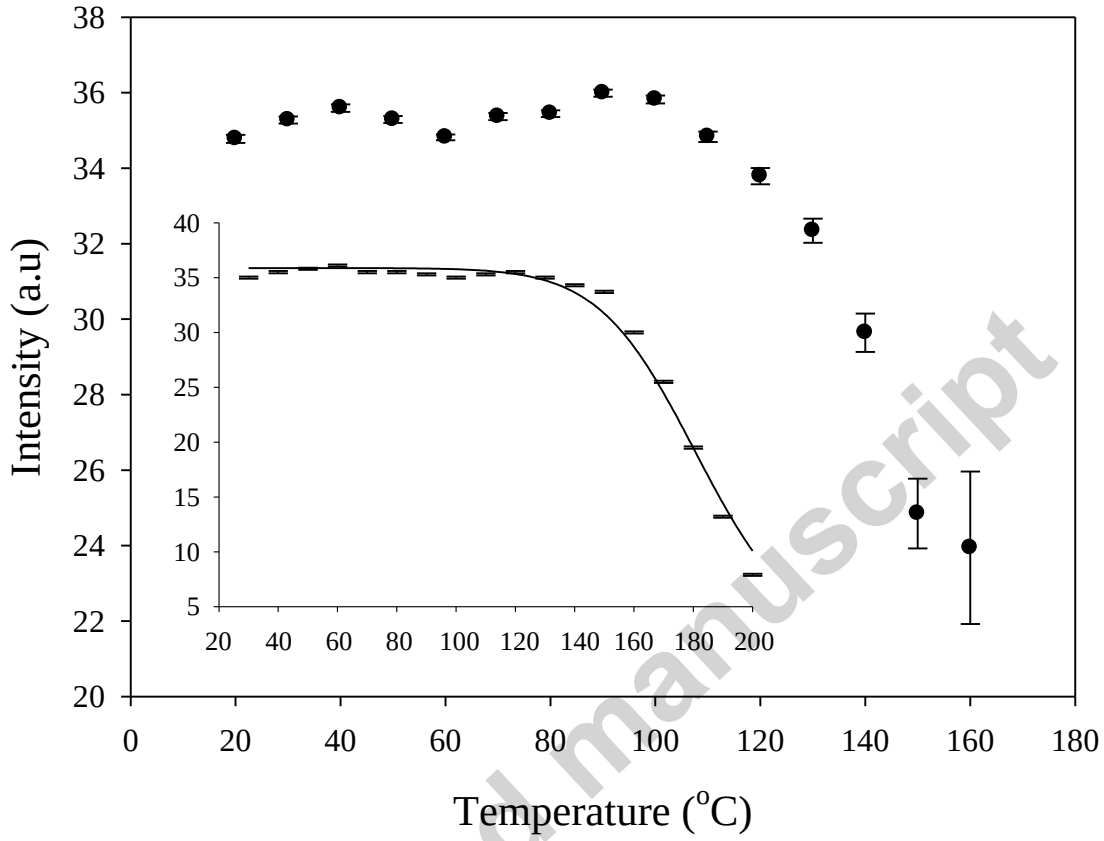

Figure 5

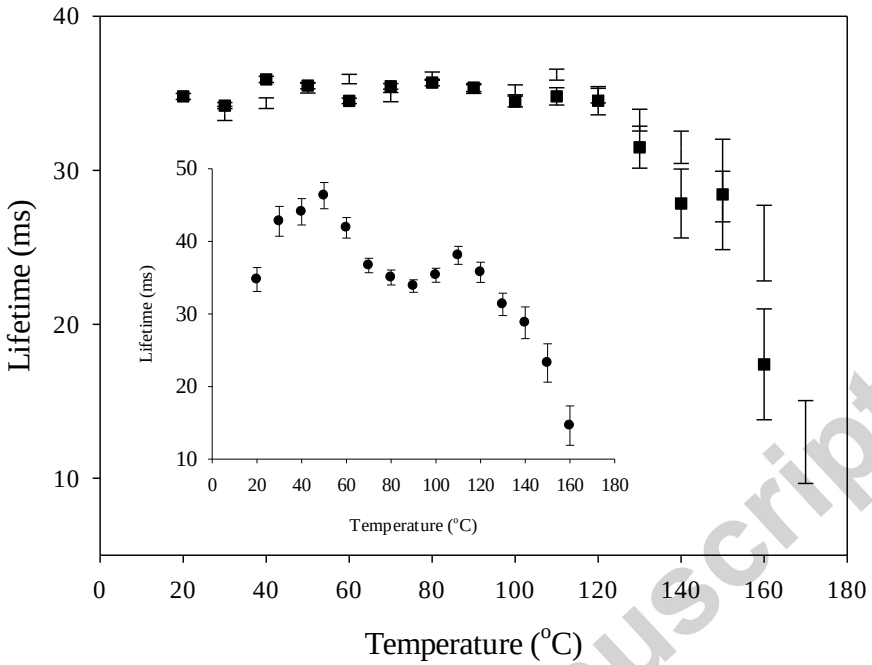

Figure 6

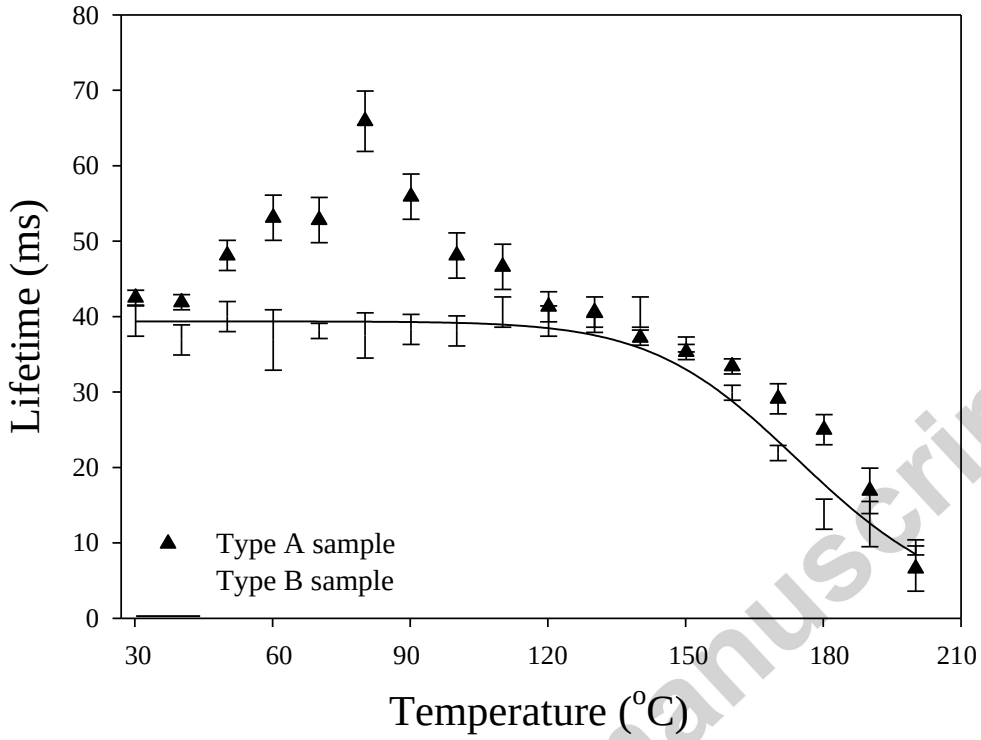

Figure 7

(a)

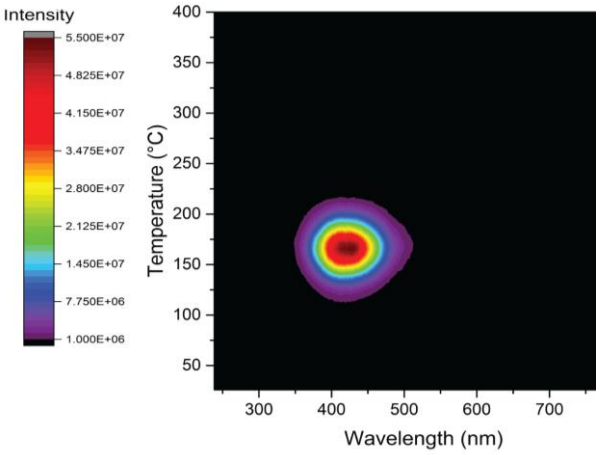
Intensity
5.500E+07
4.825E+07
4.150E+07
3.475E+07
2.800E+07
2.125E+07
1.450E+07
7.750E+06
1.000E+06
Temperature (°C)
400
350
300
250
200
150
100
50
300
400
500
600
700
Wavelength (nm)

(b)

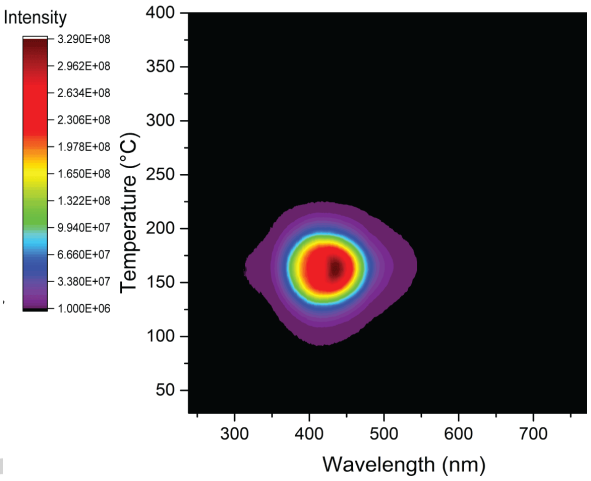
Intensity
3.290E+08
2.962E+08
2.634E+08
2.306E+08
1.978E+08
1.650E+08
1.322E+08
9.940E+07
6.660E+07
3.380E+07
1.000E+06
Temperature (°C)
400
350
300
250
200
150
100
50
300
400
500
600
700
Wavelength (nm)

(c)

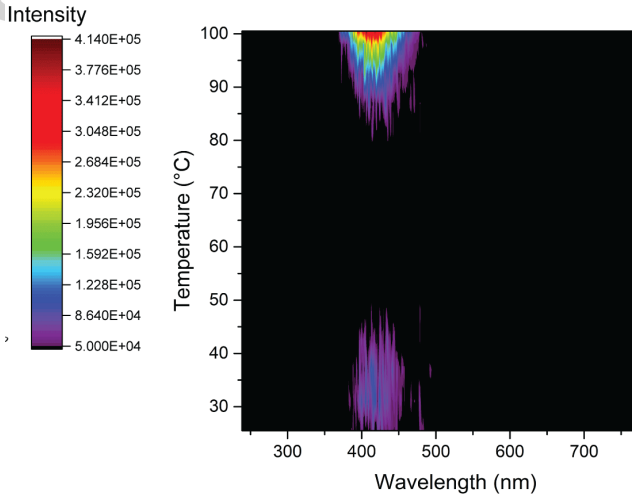
Intensity
4.140E+05
3.776E+05
3.412E+05
3.048E+05
2.684E+05
2.320E+05
1.956E+05
1.592E+05
1.228E+05
8.640E+04
5.000E+04
Temperature (°C)
100
90
80
70
60
50
40
30
300
400
500
600
700
Wavelength (nm)

Figure 8

(a)

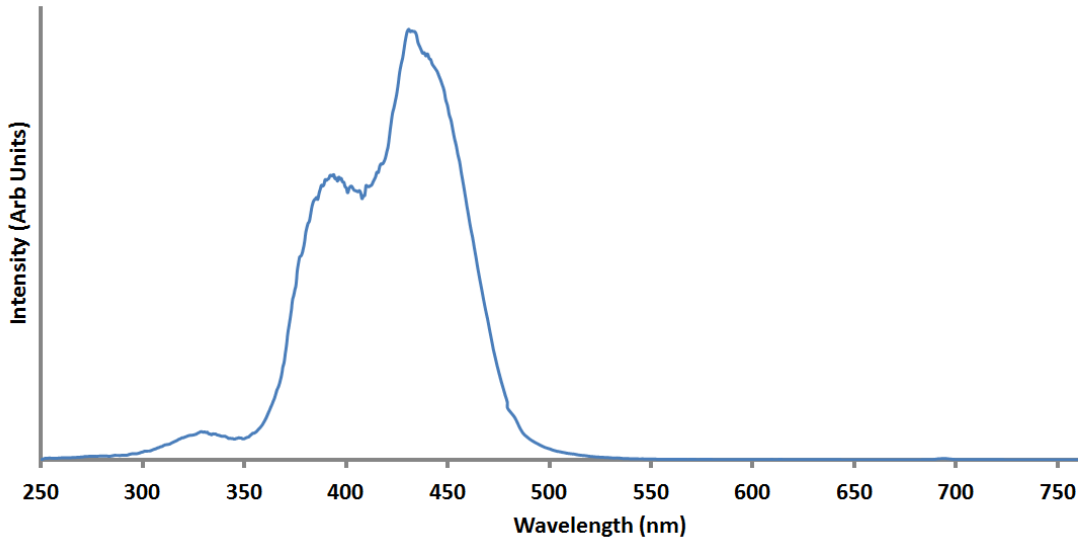
Intensity (Arb Units)
250
300
350
400
450
500
550
600
650
700
750
Wavelength (nm)

(b)

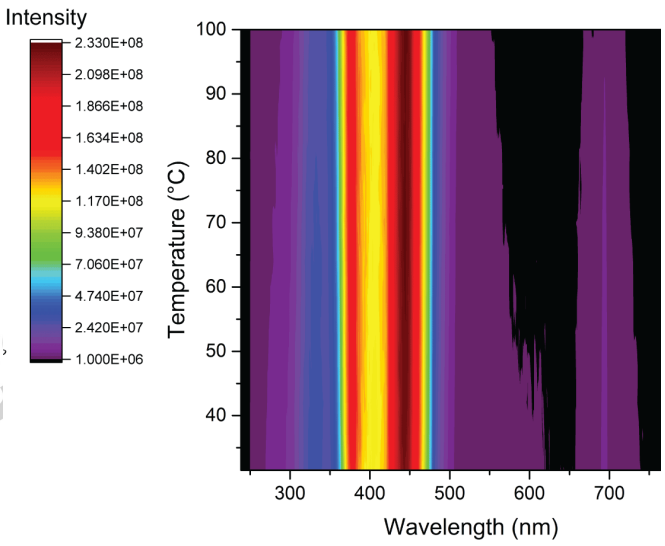
Intensity
2.330E+08
2.098E+08
1.866E+08
1.634E+08
1.402E+08
1.170E+08
9.380E+07
7.060E+07
4.740E+07
2.420E+07
1.000E+06
Temperature (°C)
100
90
80
70
60
50
40
300
400
500
600
700
Wavelength (nm)

Figure 9

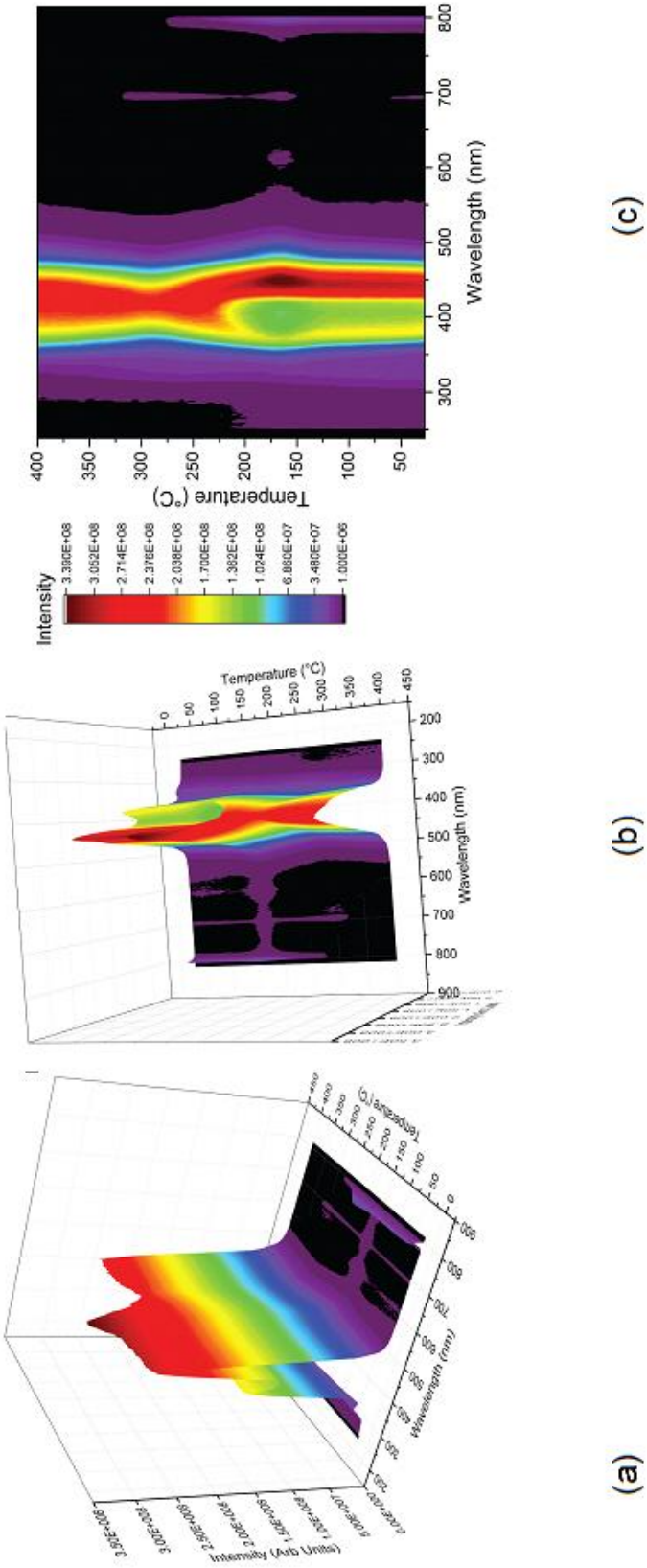
(c)
Temperature (°C)
Wavelength (nm)
Intensity
(b)
Temperature (°C)
Wavelength (nm)
(a)
Temperature (°C)
Wavelength (nm)
Intensity (Arb Units)

Figure 10

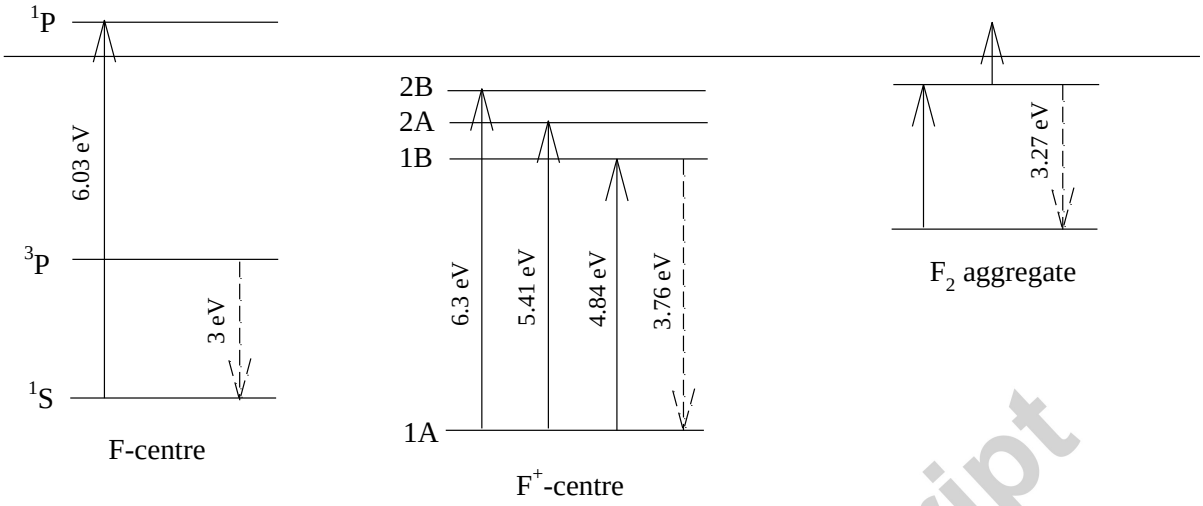

Figure 11